GMR
The Original

ANTIDIABETIC POTENTIAL OF MULTISCALE POLYMERIC ELECTROSPUN NANOSCAFFOLDS LOADED WITH CuO NANOPARTICLES FROM *Sargassum muticum* EXTRACT

Sheetal Raman Murugaiyan[1], Akilesh Anbalagan[2], Shanmugavani S[3], Alagendran Subbarayalu[4]*

[1]Saveetha Medical College & Hospital (SMCH), Saveetha Institute of Medical and Technical Sciences (SIMATS), Thandalam, Chennai, Tamil Nadu 602105, India. rmsheetal157@gmail.com
[2]Department of Anaesthesiology, Saveetha Medical College and Hospital, Saveetha Institute of Medical And Technical Sciences (SIMATS), Thandalam, Chennai-602105, Tamil Nadu, India. Email: dr.akilesh97@gmail.com; ORCID: https://orcid.org/0009-0008-3742-6538.
[3]Department of Bioinformatics, Vels Institute of Science, Technology & Advanced Studies (VISTAS), Pallavaram, Chennai, Tamil Nadu 600117, India. Email: vani.samy@gmail.com.
[4]Clinical Neuroscience and Phytomedicine Laboratory, Department of Research, Saveetha College of Nursing (SCON), Saveetha Institute of Medical and Technical Sciences (SIMATS), Chennai 602105, Tamil Nadu, India. Email: proteinblg@gmail.com; alagendrans.scon@saveetha.com. ORCID: https://orcid.org/0009-0009-0749-7180.
*Correspondence: proteinblg@gmail.com; alagendrans.scon@saveetha.com (A.S.)

ABSTRACT

This study explores the *in vitro* antidiabetic potential of starch/PVA electrospun nanoscaffolds loaded with biogenic CuO nanoparticles (NPs) synthesized from *Sargassum muticum* extract. UV-Vis spectroscopy confirmed CuO NP formation via a distinct SPR peak at 270 nm, while Fourier Transform Infrared (FTIR) and X-ray Diffraction (XRD) analyses verified their structural integration into nanoscaffolds, revealing key functional groups and monoclinic crystallinity (JCPDS 05-0661). Scanning Electron Microscopy (SEM) imaging showed uniform NP dispersion within a porous fibrous network (100–150 nm diameter), and Thermogravimetric Analysis (TGA) demonstrated thermal stability up to 243°C. The CuO NPs exhibited moderate colloidal stability (zeta potential: −12.62 mV; size: 92.1 nm). In antidiabetic assays, the nanoscaffolds outperformed both algal extract and standalone CuO NPs, achieving 80.42% α-amylase and 79.32% α-glucosidase inhibition at 100 µg/mL, nearing the efficacy of acarbose. The dose-dependent inhibition highlights synergistic effects between CuO NPs and the polymer matrix, suggesting enhanced bioactive delivery. These findings position starch/PVA/CuO-NP nanoscaffolds as a promising platform for diabetes therapy, warranting further *in vivo* validation.

KEYWORDS: *Sargassum muticum*, Green synthesis, CuO NPs, Starch/PVA-nanoscaffolds, Antidiabetic activity.

1. INTRODUCTION

Diabetes mellitus (DM) is a chronic metabolic disorder characterized by hyperglycemia resulting from defects in insulin secretion, insulin action, or both [1]. Globally, the burden of diabetes is escalating at an alarming rate, affecting over 537 million adults according to the International Diabetes Federation (IDF), with projections suggesting this number may rise to 783 million by 2045 [2]. The disease is associated with a multitude of complications, including cardiovascular diseases, nephropathy, neuropathy, and retinopathy, which severely impact the quality of life and impose significant economic and healthcare burdens [3]. Current pharmacological interventions for diabetes, including insulin therapy and oral hypoglycemics such as sulfonylureas, biguanides, and α-glucosidase inhibitors, often exhibit limitations like gastrointestinal discomfort, hypoglycemia, and long-term inefficacy [4]. Consequently, there is a pressing need for safer, more effective, and sustainable alternatives derived from natural sources [5].

In recent years, marine-derived resources have emerged as a prolific reservoir of bioactive compounds with potential antidiabetic activities [6]. Among them, brown macroalgae (*Phaeophyceae*) are especially significant due to their abundance in phenolic compounds, polysaccharides, and flavonoids with proven pharmacological properties [7]. *Sargassum muticum*, a widely distributed brown macroalga, has attracted scientific interest due to its therapeutic properties, including antioxidant, anti-inflammatory, antibacterial, and antidiabetic activities [8]. Extracts from *S. muticum* are rich in phlorotannins, alginates, fucoidans, and other polyphenols known to modulate glucose metabolism, inhibit digestive enzymes, and enhance insulin sensitivity [9]. Despite its bioactive potential, *S. muticum* remains underexplored in nanobiotechnology-based diabetes interventions.

Nanotechnology has transformed biomedical sciences by offering new paradigms in drug delivery, diagnostics, and therapeutics [10]. Metal oxide nanoparticles (NPs), particularly copper oxide nanoparticles (CuO NPs), have

emerged as promising agents due to their excellent biocompatibility, cost-effectiveness, and multifaceted bioactivities [11]. CuO NPs have demonstrated significant antibacterial, antioxidant, anticancer, and antidiabetic properties [12]. Their ability to inhibit α-amylase and α-glucosidase enzymes, key players in postprandial hyperglycemia, underlines their therapeutic relevance in diabetes management [13]. However, conventional chemical synthesis routes often involve toxic reagents and generate hazardous by-products, limiting their applicability in biomedical contexts [14].

To address this limitation, green synthesis techniques employing biological entities have garnered attention as eco-friendly and sustainable alternatives [15]. Marine algae-mediated synthesis offers a cost-effective, scalable, and non-toxic approach to produce NPs with enhanced stability and biological functionality [16]. The phytochemicals in *S. muticum*, including hydroxyl and carboxyl groups, serve as natural reducing and stabilizing agents, facilitating the formation of CuO NPs with desirable physicochemical properties [17]. Moreover, coupling ultrasonic-assisted extraction with green synthesis further improves the yield and bioavailability of active constituents by enhancing cellular disruption and diffusion of phytochemicals through cavitation effects [18].

Alongside nanomaterials, electrospun nanofibrous scaffolds have emerged as innovative platforms for controlled drug delivery and tissue engineering applications [19]. Electrospinning enables the fabrication of nanofibers with high surface area-to-volume ratios, porosity, and ECM-mimicking architectures, offering substantial advantages in biomedical applications [20]. Blending starch, a biodegradable and biocompatible natural polymer, with synthetic polymers like polyvinyl alcohol (PVA) can result in nanocomposite scaffolds with superior mechanical and physiological properties [21]. Starch offers bioactivity and biodegradability, while PVA contributes to structural integrity and fiber formation during electrospinning [22].

The integration of bioactive CuO NPs into starch/PVA nanofibrous scaffolds offers a promising strategy for developing functional biomaterials with antidiabetic capabilities [23]. Such nanocomposites not only provide a matrix for sustained and targeted delivery of therapeutic agents but also facilitate direct enzyme inhibition through surface interaction [24]. Furthermore, the synergistic effect of plant-derived CuO NPs and biopolymer matrices can improve therapeutic outcomes while minimizing side effects commonly associated with synthetic drugs [25].

Despite these promising features, studies on the in vitro antidiabetic potential of electrospun nanoscaffolds embedded with green-synthesized CuO NPs, particularly those derived from *S. muticum*, are scarce. The novelty of the present study lies in the eco-friendly synthesis of CuO NPs using ultrasonic-assisted *S. muticum* extract and their subsequent incorporation into starch/PVA electrospun nanoscaffolds. This research aims to bridge the gap between marine biotechnology and nanomedicine by evaluating the dual role of these composite scaffolds in structural support and enzymatic inhibition for diabetes therapy.

2. MATERIALS AND METHODS

2.1. Collection and processing of marine macroalgae

Fresh samples of whole *S. muticum* were manually gathered from the intertidal coastal regions surrounding Rameswaram, Tamil Nadu, India. The collected *Sargassum muticum* was taxonomically identified and authenticated by Dr V. Veeragurunathan, CSIR-CSMCRI-Marine Algal Research Station, Mandapam Camp 623519, Tamil Nadu, India. A voucher specimen was prepared and deposited at the Herbarium of the CSIR-CSMCRI-Marine Algal Research Station, under the accession number: SI–2025–RMM–016. This authentication ensures botanical accuracy and standardization of the study material. The collected specimens were transported to the laboratory in chilled containers to maintain freshness. Initially, the algal biomass was rinsed with tap water to eliminate sand, debris, and any surface epiphytes, followed by repeated washes using distilled water to ensure all impurities were removed. The cleaned algae were chopped into smaller segments and left to air-dry in a shaded, well-ventilated environment at room temperature for about 14 days. Once dried, the algal material was pulverized into a fine powder using a mechanical grinder and stored in sealed containers at ambient temperature until required for extraction.

2.2. Extraction of bioactive components via ultrasonication

To isolate phytochemicals from *S. muticum*, 2 grams of the dried powdered sample were mixed with 50 mL of Milli-Q water and subjected to ultrasonic-assisted extraction using a LABQUEST ultrasonic cleaner (Borosil; Serial No. 941032329018). The process was carried out at 60°C for a total duration of 45 minutes, facilitating enhanced release of active compounds via cavitation. The resulting mixture was filtered through Whatman No. 1 filter paper under sterile conditions to obtain a clear solution. The extract was immediately stored at 10°C and subsequently freeze-dried using a lyophilizer for prolonged storage and subsequent applications [26].

2.3. Eco-Friendly synthesis of CuO NPs

The synthesis of CuO NPs was initiated by combining 50 mL of a 0.1 M $CuSO_4 \cdot 5H_2O$ aqueous solution with 10 mL of *S. muticum* extract (prepared by dissolving 10 mg of the lyophilized powder in 10 mL of Milli-Q water) in

a 5:1 volume ratio. This mixture was stirred continuously at 650 rpm and heated to 60°C for a period of 2 hours. A visual change in color from blue to bluish-green was observed, signifying the formation of CuO NPs through the reduction of copper ions. The resultant mixture was centrifuged and rinsed thrice with double-distilled water to remove any residual plant compounds and unreacted materials. The final nanoparticle product was freeze-dried over 48 hours and preserved in a desiccated chamber for further analysis and scaffold fabrication [27].

2.4. Fabrication of starch/PVA nanofibrous scaffolds with embedded CuO NPs

To develop nanocomposite scaffolds, a 15% (w/w) solution of PVA was prepared in Milli-Q water with continuous agitation until fully dissolved. To this solution, 100 mg each of starch and green-synthesized CuO NPs were added. The mixture was stirred rigorously at 50°C for 2.5 hours to ensure uniform dispersion. The resulting solution was then loaded into a syringe fitted with a stainless-steel needle (0.84 mm internal diameter) and mounted on a HOLMARC HO-NFES-040 electrospinning system. Optimal parameters were set at an applied voltage of 11.5 kV, needle-to-collector distance of 12.3 cm, and a feed rate of 0.4 mL/h. Electrospinning was performed at room temperature for 6 to 8 hours, yielding nanofibrous mats. These were carefully removed and stored in a desiccator for further characterization [28-30].

2.5. Physicochemical analysis of NPs and electrospun mats

2.5.1. UV-Visible spectroscopy

The optical behavior of both the CuO NPs and *S. muticum* extract was assessed using a VIS SPEC V-730 spectrophotometer, scanning from 200 to 800 nm. Deionized water served as the baseline. The presence of surface plasmon resonance (SPR) peaks indicated successful nanoparticle formation [31].

2.5.2. Fourier Transform Infrared (FTIR) spectroscopy

FTIR measurements were conducted in attenuated total reflectance (ATR) mode utilizing the PerkinElmer Spectrum Two system. Spectral data were collected in the range of 4000 to 400 cm^{-1} at 4 cm^{-1} resolution with 64 scans per sample. The spectral peaks corresponding to functional groups such as hydroxyl, phenolic, carbonyl, and metal-oxygen were analyzed [32].

2.5.3. X-ray Diffraction (XRD) analysis

Crystalline structure and phase identification of CuO NPs and nanofibrous composites were performed using a Bruker D8 Advance diffractometer with CuKα radiation (λ = 1.5406 Å), operating at 40 kV and 40 mA. Diffraction data were collected over a 2θ range of 5° to 90°, with a 0.029649° step interval. The diffraction peaks were matched with JCPDS reference standards for CuO confirmation [33].

2.5.4. Scanning Electron Microscopy (SEM)

The surface morphology and particle distribution within the scaffolds and NPs were observed using a JEOL JSM-IT800 NANO SEM. Prior to imaging, samples were coated with a thin gold layer using a sputter coater to improve electron conductivity. SEM images were analyzed for fiber thickness, particle incorporation, and surface texture [34].

2.5.5. Thermogravimetric Analysis (TGA)

Thermal properties and degradation trends of the nanocomposites were studied using a PerkinElmer TGA 8000 analyzer. Approximately 5 mg of each sample was heated from room temperature to 550°C at a rate of 15°C/min under a nitrogen atmosphere. The TGA thermograms provided data on moisture content, polymer decomposition, and final residue weight [35, 36].

2.5.6. Zeta potential and particle size measurement

The particle size distribution and surface charge of the synthesized CuO NPs were determined using the Malvern Zetasizer Ultra. Zeta potential readings were used to evaluate particle stability in suspension, where a high absolute value suggested strong electrostatic repulsion and good colloidal stability [37].

All experimental data and analysis results are available in the Mendeley Data repository, accessible via DOI: 10.17632/jrs2y2hp7v.2.

2.6. Evaluation of antidiabetic activity

2.6.1. α-Amylase inhibition assay

The inhibitory effect of the algal extract, CuO NPs, and starch/PVA/CuO-NPs nanocomposite against α-amylase was assessed using a modified dinitrosalicylic acid (DNSA) method. Each test involved mixing 200 µL of α-amylase solution (1 U/mL) with 200 µL of the test samples at concentrations of 25, 50, 75, and 100 µg/mL. After

pre-incubation at 37°C for 10 minutes, 200 µL of 1% starch in 0.02 M sodium phosphate buffer (pH 6.9) was added. The reaction was continued at 37°C for 30 minutes, followed by termination using 400 µL of DNSA reagent and heating for 5 minutes. Absorbance was read at 540 nm to measure reducing sugar formation. Acarbose was used as a standard, and IC_{50} values were computed using non-linear regression plots of percentage inhibition [38].

2.6.2. α-Glucosidase inhibition assay

The α-glucosidase inhibitory activity of various samples, including Sargassum extract, CuO NPs, and CuO-loaded starch/PVA scaffolds, was evaluated using a colorimetric method. Each reaction consisted of 50 µL of α-glucosidase enzyme (1 U/mL) mixed with 50 µL of test samples at different concentrations (25–100 µg/mL) and incubated at 37°C for 15 minutes. Subsequently, 50 µL of 5 mM p-nitrophenyl-α-D-glucopyranoside (pNPG) in phosphate buffer (pH 6.8) was added to initiate the enzymatic reaction, followed by a 30-minute incubation. The reaction was stopped with 100 µL of 0.1 M sodium carbonate, producing a yellow color from released p-nitrophenol. Absorbance was measured at 405 nm. Acarbose was employed as a control, and IC_{50} values were derived through non-linear regression analysis to determine the formulation's potency [39, 40].

2.7. Statistical analysis

Data obtained from the experiments were subjected to statistical evaluation using SPSS version 25.0 and GraphPad Prism 9.0 software. All measurements were conducted in triplicate and expressed as mean ± standard deviation. One-way ANOVA was applied to identify significant differences between groups, followed by Tukey's or Dunnett's post-hoc tests as applicable. A p-value of less than 0.05 was considered statistically significant. The Shapiro-Wilk test was employed to confirm normal distribution of data, and in cases of non-normality, logarithmic transformations were carried out. Pearson correlation coefficients were computed to evaluate relationships between variables. All results were interpreted within a 95% confidence level to ensure robust and reliable conclusions [41].

3. RESULTS

3.1. UV–visible spectroscopy

UV-Vis spectroscopic analysis (Fig. 1) of *S. muticum* extract and CuO NPs was performed using a JASCO V-730 spectrophotometer (200–800 nm, 1 nm interval). The extract displayed absorption patterns typical of phytochemicals, while CuO NPs exhibited a distinct surface plasmon resonance (SPR) peak at 270 nm, confirming nanoparticle formation. Absorbance measurements (0.477617 at 270 nm) validated successful synthesis. Instrument parameters (1.0 nm bandwidth, 1000 nm/min scan speed, continuous filter exchange) ensured high-resolution data. The results highlight the optical differences between the extract and CuO NPs, with the latter's SPR signature confirming its nanoscale properties.

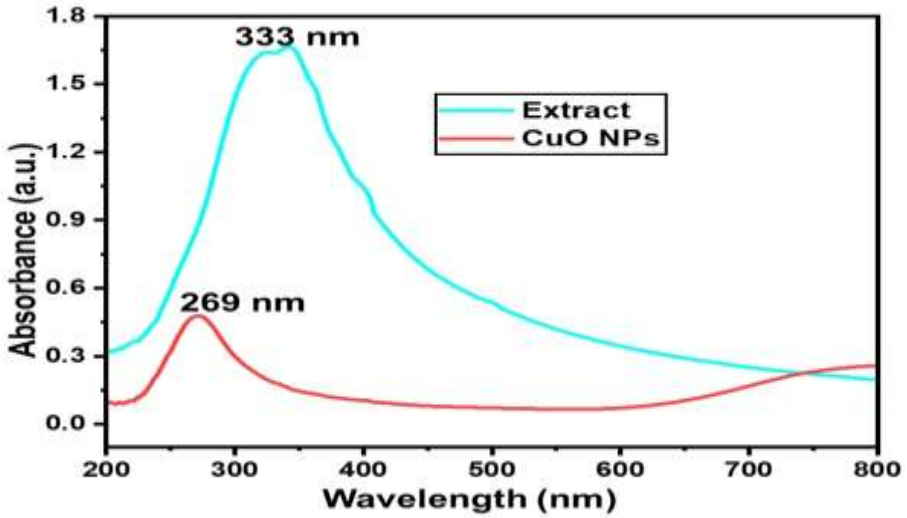

Fig. 1. UV–Visible spectral profiles of algal extract and CuO NPs.

3.2. FTIR spectroscopy

FTIR spectra (Fig. 2) of CuO NPs and starch/PVA nanoscaffolds (PerkinElmer Spectrum Two, ATR mode, 4000–400 cm^{-1}, 4 cm^{-1} resolution) revealed key functional groups. CuO NPs showed O–H stretching at 3277.29 cm^{-1} and C–H/carbonyl interactions at 2700.50 cm^{-1} and 2500.00 cm^{-1}. The nanoscaffolds exhibited C=O stretching (1500.00 cm^{-1}) and glycosidic linkages (840.00 cm^{-1}), while peaks below 1000 cm^{-1} (e.g., 600.00 cm^{-1})

confirmed Cu–O bonds, verifying NP incorporation. These findings demonstrate the scaffold's structural integrity and successful integration of CuO NPs.

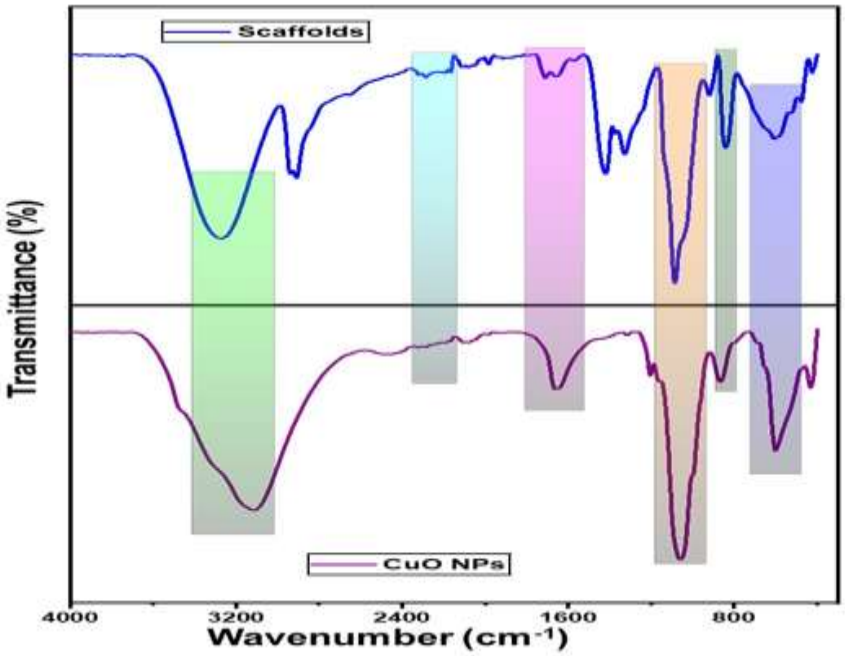

Fig. 2. FTIR spectra of CuO NPs and their incorporation into nanoscaffolds.

3.3. XRD analysis

XRD (Fig. 3) (Bruker D8 Advance, CuKα radiation, 5°–90° 2θ) confirmed monoclinic CuO NPs with peaks at 32.745° (110), 35.297° (002), 38.307° (111), and 48.123° (202) (JCPDS 05-0661). Starch/PVA scaffolds showed semicrystalline peaks at 19.270°, 21.364°, and 23.525°, with additional reflections (26.536°, 29.481°) indicating CuO NP interactions. The d-spacing (2.732 Å for CuO NPs; 4.602 Å for scaffolds) and relative intensities confirmed crystallinity differences, validating phase-pure CuO NPs and their dispersion in the polymer matrix.

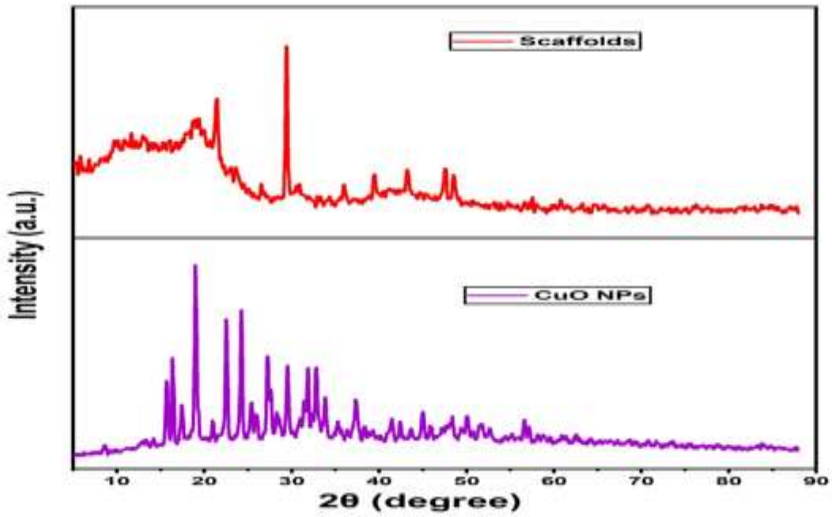

Fig. 3. XRD patterns of synthesized CuO NPs and CuO-loaded scaffolds.

3.4. SEM analysis

SEM (JEOL JSM-IT800 NANO) (Fig. 4) revealed CuO NPs as spherical/irregular aggregates, while starch/PVA scaffolds formed a porous, fibrous network (100–150 nm diameter). Uniform NP dispersion on fiber surfaces confirmed effective incorporation. The scaffolds' high porosity and smooth morphology (with minor beading) suggest suitability for biomedical applications requiring high surface area and structural integrity.

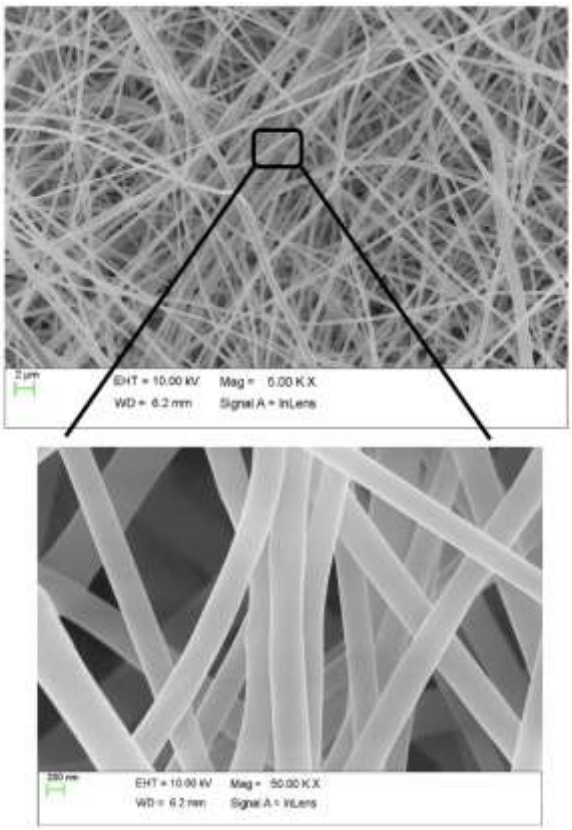

Fig. 4. SEM analysis of synthesized CuO NPs and CuO-loaded scaffolds.

3.5. TGA

Thermogravimetric analysis (Fig. 5) (PerkinElmer, N_2 atmosphere, 25–550°C) showed scaffold decomposition in stages: moisture loss (<150°C), polymer breakdown (onset: 243.01°C; peak: 349.62°C), and residual mass (51.881%). The sharp decline (200–400°C) reflected starch/PVA degradation, while the high residue suggested crosslinking or inorganic content, indicating thermal stability up to 243°C.

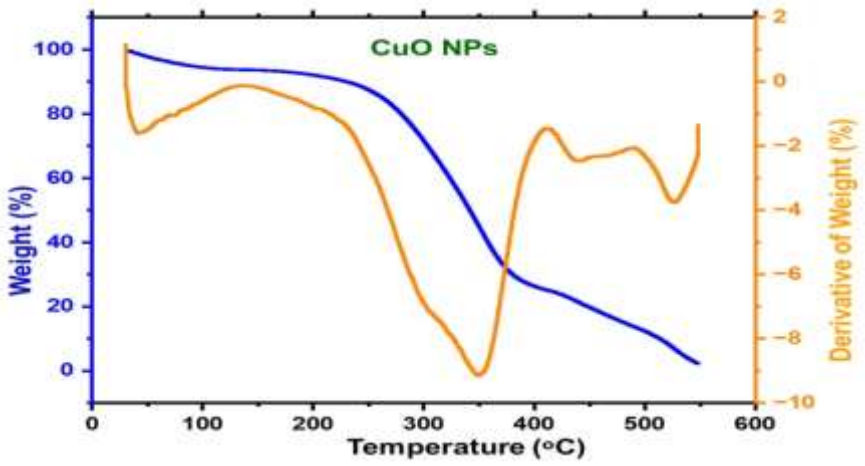

Fig. 5. Thermal degradation behavior of CuO-incorporated nanoscaffolds.

3.6. Zeta potential and particle size analysis

DLS (Malvern Zetasizer Ultra) revealed CuO NPs with a 92.1 nm Z-average size (Fig. 6) and PDI of 0.8444, indicating moderate polydispersity. Zeta potential (−12.62 mV, peaks at −20.85 mV and −8.994 mV) (Fig. 7) suggested colloidal stability via electrostatic repulsion. Conductivity (0.07909 mS/cm) and quality factor (5.109) supported measurement reliability, highlighting the NPs' moderate stability in suspension.

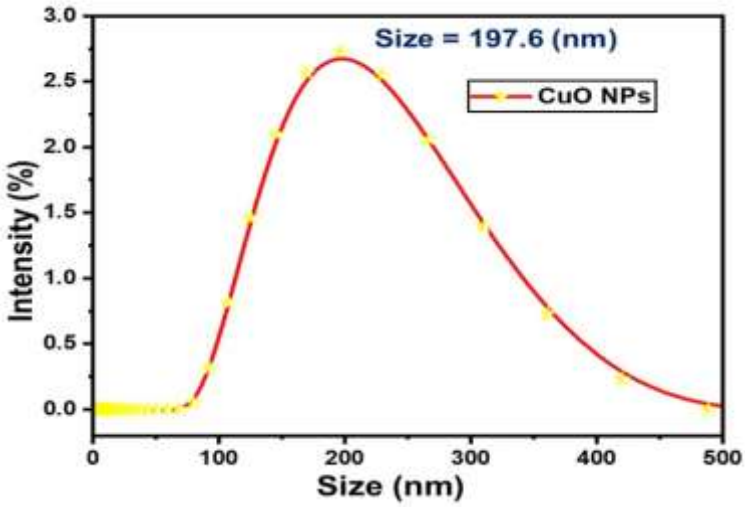

Fig.6. DLS particles size analysis of CuO NPs

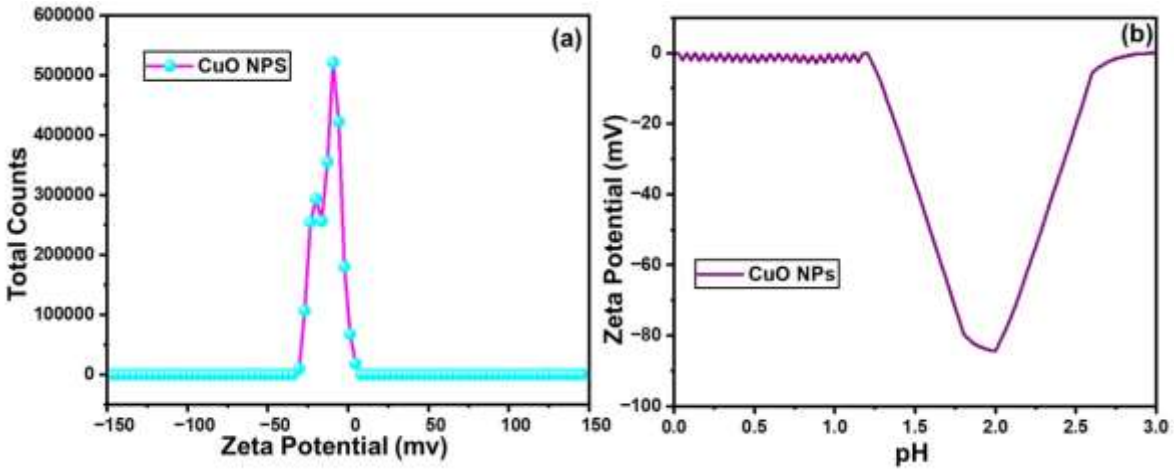

Fig.7. Zeta-potential analysis of CuO NPs

3.7. In vitro antidiabetic activity

The antidiabetic potential of algal extract, CuO NPs, and starch/PVA/CuO-NPs nanoscaffolds was evaluated through their inhibitory effects on α-amylase and α-glucosidase enzymes, key targets for managing postprandial hyperglycemia.

3.7.1. α-Amylase inhibition

The algal extract demonstrated moderate α-amylase inhibition (Fig. 8), with percentages ranging from 19.22% at 25 µg/mL to 51.42% at 100 µg/mL. CuO NPs exhibited stronger inhibition, increasing from 21.22% (25 µg/mL) to 69.42% (100 µg/mL), suggesting enhanced enzyme-blocking activity compared to the crude extract. Notably, the composite nanoscaffolds (starch/PVA/CuO-NPs) displayed the highest efficacy, nearing the standard drug acarbose (81.34% at 100 µg/mL), with inhibition rates of 24.22% (25 µg/mL) rising sharply to 80.42% (100 µg/mL). This indicates that the nanoscaffold's structural formulation significantly boosts α-amylase suppression, potentially due to improved stability or synergistic interactions between CuO NPs and the polymer matrix.

3.7.2. α-Glucosidase inhibition

In the α-glucosidase assay (Fig. 8), the algal extract showed lower inhibition (15.12–51.32%) across the tested concentrations (25–100 µg/mL). CuO NPs again outperformed the extract, achieving 17.12–66.32% inhibition, while the nanoscaffolds reached 24.12–79.32%, closely mirroring acarbose's performance (28.13–84.34%). The nanoscaffold's superior activity may stem from controlled release or enhanced enzyme-binding affinity, underscoring its potential as a multifunctional antidiabetic agent.

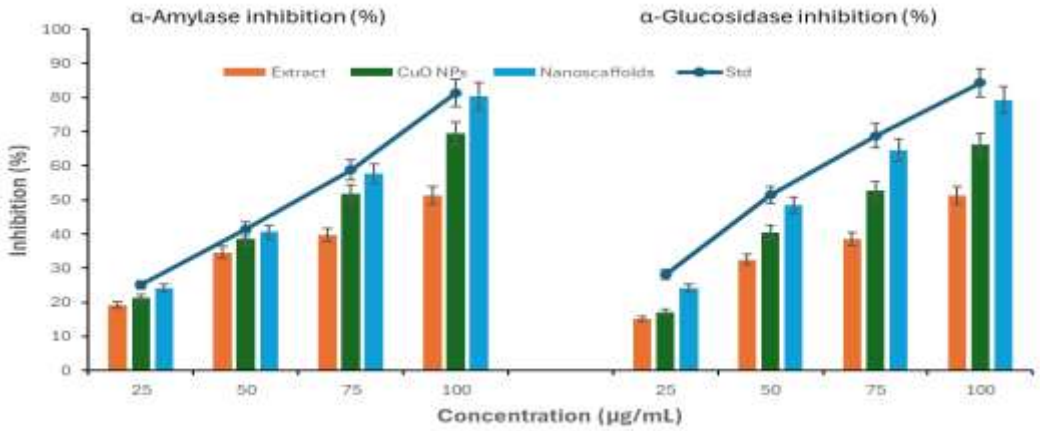

Fig.8. Antidiabetic activity analysis of algal extract, CuNPs and starch/PVA/CuONPs nanoscaffolds

Both assays revealed a dose-dependent response for all samples. The nanoscaffolds consistently exhibited the highest inhibition, likely due to the combined effects of CuO NPs' catalytic properties and the polymer matrix's biocompatibility. While the algal extract showed baseline activity, its lower efficacy highlights the need for nanoformulation to optimize therapeutic outcomes. These findings align with literature on nanostructured systems enhancing bioactive compound delivery and enzyme inhibition.

The starch/PVA/CuO-NPs nanoscaffolds emerged as the most promising candidate, with inhibition profiles rivaling acarbose. Further studies should focus on IC_{50} determination and in vivo validation to confirm their clinical applicability in diabetes management.

4. DISCUSSION

The characterization and evaluation of the *S. muticum*-mediated CuO NPs and their incorporation into starch/ PVA electrospun nanoscaffolds provide compelling evidence of their successful synthesis, structural integrity, and potential biomedical applicability. Each analytical technique used in this study contributed critical insights into the physicochemical, morphological, and biological profiles of the NPs and the composite scaffolds.

UV–Visible spectroscopy served as the initial confirmatory tool for nanoparticle formation. The S. *muticum* extract exhibited broad absorption bands in the UV region, which is characteristic of natural phytochemicals such as polyphenols, flavonoids, and terpenoids. These compounds are often responsible for reducing metal ions and stabilizing the resulting NPs. In contrast, the UV–Vis spectrum of the synthesized CuO NPs displayed a distinct surface plasmon resonance (SPR) peak at 270 nm. This sharp peak is indicative of successful nanoparticle synthesis and is consistent with reported SPR values for CuO NPs, confirming the presence of uniformly dispersed CuO NPs with characteristic optical properties. The absorbance value of 0.477617 at 270 nm further validated the stability and uniformity of the nanoparticle suspension. Instrumental parameters—such as a 1.0 nm bandwidth, 1000 nm/min scanning speed, and continuous filter exchange—contributed to the acquisition of high-resolution spectral data. These findings clearly differentiate the optical behavior of the crude extract and the synthesized NPs, establishing UV–Vis spectroscopy as a reliable and rapid characterization tool [42-48].

FTIR spectroscopy provided insights into the chemical functionalities associated with both CuO NPs and starch/PVA-based nanoscaffolds. The FTIR spectrum of CuO NPs demonstrated an intense peak at 3277.29 cm^{-1} corresponding to O–H stretching vibrations, indicative of hydroxyl groups likely originating from capping agents in the algal extract. Peaks at 2700.50 cm^{-1} and 2500.00 cm^{-1} are attributed to C–H stretching and possible carbonyl interactions, suggesting the presence of residual organic molecules from the biological synthesis process. In the nanoscaffold spectrum, the presence of strong C=O stretching vibrations around 1500.00 cm^{-1} confirmed successful incorporation of the polymer matrix, while peaks at 840.00 cm^{-1} pointed to glycosidic bonds from starch. Notably, characteristic Cu–O stretching vibrations observed near 600.00 cm^{-1} affirmed the successful embedding of CuO NPs within the polymer framework. This dual characterization confirms both the chemical integrity of the scaffold and the stability of the embedded NPs [49-54].

XRD analysis played a pivotal role in confirming the crystallinity and phase purity of the synthesized NPs and their incorporation into the composite scaffold. The CuO NPs exhibited sharp diffraction peaks at 2θ values of 32.745°, 35.297°, 38.307°, and 48.123°, corresponding to the (110), (002), (111), and (202) planes of monoclinic CuO, in accordance with JCPDS 05-0661. These sharp reflections indicate well-crystallized NPs. In contrast, the XRD pattern of the starch/PVA nanoscaffolds presented broader, semicrystalline peaks around 19.270°, 21.364°, and 23.525°, which are typical for polymer blends. Additional minor peaks at 26.536° and 29.481° were attributed

to CuO NP integration, suggesting successful physical dispersion within the matrix. The measured d-spacing of 2.732 Å for CuO NPs and 4.602 Å for scaffolds revealed structural differences between the inorganic and polymeric phases. These results collectively support the conclusion that phase-pure CuO NPs were successfully integrated into the nanoscaffold without compromising crystallinity [55-59].

SEM imaging offered crucial visual confirmation of morphology and nanoparticle integration. The CuO NPs appeared as mostly spherical to irregular aggregates, a morphology consistent with biologically synthesized metal oxide NPs. The starch/PVA nanoscaffolds exhibited a highly porous, fibrous network with fiber diameters ranging from 100 to 150 nm. The fibers displayed a smooth surface with occasional bead formations, typical of optimized electrospinning processes. More importantly, the SEM micrographs showed well-dispersed CuO NPs embedded on or within the fibrous matrix, confirming successful nanoparticle incorporation. The high porosity and fiber uniformity are desirable traits for biomedical scaffolds, supporting their potential in applications requiring high surface area and interfacial interactions, such as drug delivery or tissue regeneration [60-64].

The TGA profile of the composite scaffolds revealed multi-step thermal degradation. Initial weight loss below 150°C was attributed to the evaporation of physically adsorbed moisture. The subsequent major degradation phase, beginning at 243.01°C and peaking at 349.62°C, corresponded to the decomposition of the polymer components, namely starch and PVA. The total residual mass was 51.881%, indicating a substantial amount of non-volatile inorganic content—most likely CuO NPs and crosslinked residues—contributing to thermal stability. The results suggest that the nanoscaffolds are thermally stable up to approximately 243°C, a feature beneficial for potential sterilization and biomedical use [65-69].

Zeta potential and DLS analyses provided information on the colloidal properties of the CuO NPs. The hydrodynamic diameter was measured at 92.1 nm with a polydispersity index (PDI) of 0.8444, suggesting a moderately polydisperse system. The zeta potential value of −12.62 mV, with peaks at −20.85 mV and −8.994 mV, reflects moderate colloidal stability, governed primarily by electrostatic repulsion among negatively charged particles. The conductivity value of 0.07909 mS/cm and a high quality factor (5.109) supported the reliability and reproducibility of these measurements. While the zeta potential falls short of the ideal ±30 mV range for strong colloidal stability, the values obtained are adequate for biological applications involving transient interactions [70, 71].

The antidiabetic potential was assessed using α-amylase and α-glucosidase inhibition assays. The S. *muticum* extract exhibited moderate inhibition activity, but this was significantly enhanced upon nanoparticle synthesis. CuO NPs demonstrated stronger inhibition profiles, likely due to their nanoscale size and surface activity, which facilitate better interaction with enzyme active sites. Remarkably, the starch/PVA/CuO nanoscaffolds exhibited the highest inhibition values for both enzymes, approaching those of the standard antidiabetic drug acarbose. For α-amylase, inhibition rose from 24.22% to 80.42%, while for α-glucosidase it ranged from 24.12% to 79.32% across concentrations of 25 to 100 µg/mL. These results suggest synergistic effects between the polymeric matrix and the NPs, possibly via improved bioavailability, sustained release, or enhanced enzyme binding affinity. The consistent, dose-dependent activity confirms the scaffold's therapeutic potential [72, 73].

5. CONCLUSION

The present study successfully demonstrates the green synthesis of CuO NPs using *S. muticum* extract and their effective incorporation into starch/PVA-based nanoscaffolds. UV–Vis spectroscopy confirmed nanoparticle formation through distinct surface plasmon resonance at 270 nm, while FTIR and XRD analyses validated the structural and chemical integrity of both NPs and the composite scaffold. SEM imaging revealed a uniform, porous nanofibrous structure suitable for biomedical applications. TGA results confirmed thermal stability up to 243°C, and zeta potential analysis indicated moderate colloidal stability. Most notably, the starch/PVA/CuO-NPs nanoscaffolds exhibited significant in vitro antidiabetic activity, with potent inhibition of both α-amylase and α-glucosidase enzymes, outperforming the algal extract and CuO NPs alone. These findings underscore the potential of the synthesized nanoscaffold as a multifunctional therapeutic platform for diabetes management. Future research should include IC_{50} analysis and in vivo studies to further validate its efficacy and clinical applicability.

Ethics declaration: Not Applicable

Conflicts of Interest: The authors declare no conflicts of interest.

Data Availability Statement: The full dataset of physiochemical characterization associated with this work is published in Mendeley Data **[Dataset]** Bioactive nanostructured platforms: Physicochemical assessment of starch scaffolds hybridized with *Sargassum muticum*-copper oxide nanoparticles (DOI: 10.17632/jrs2y2hp7v.2). Disclosure: The material characterization data and figures (e.g., UV, SEM, FTIR, XRD, TGA, Zeta Potential and particle sizer) presented here were generated from a common dataset and are being reused across multiple related studies on nanomaterials. All biological analyses and conclusions are original to each manuscript.

REFERENCE

[1] Surendran N, Chandrasekaran G, Raju MV, Chandrasekaran MK, Ahalliya RM, Palanisamy CP, Kanniappan GV, Arcot R, Alharbi NS, Thiruvengadam M. Anti-inflammatory potential of ethanolic extract of Maranta arundinacea L.: Insights from COX-2 modulation and oxidative stress analysis. South African Journal of Botany. 2026; 195: 142-151.

[2] Pei J, Senthilkumar MV, Hessini K, Subramaniyam S, Sivaramakrishnan R, Kanniappan GV, Jayaraman S, Palanisamy CP. Green fabrication of starch/PVA/CuO nanoscaffolds using marine macroalgae extract for enhanced anti-inflammatory activity. Sustainable Chemistry and Pharmacy. 2026; 51: 102397.

[3] Balasubramanian V, Loganathan L, Muthuswamy K, Viswanathan TM, Raju MV, Chandrasekaran MK, Ahalliya RM, Poorasamy J, Palanisamy CP, Dominic S, Kanniappan GV. Anticancer therapeutic efficacy of PEGylated β-galactosidase from Aspergillus terreus in DMBA-induced breast cancer: Toxicological, molecular and histopathological evaluation in Wistar rats. International Journal of Biological Macromolecules. 2026; 360: 151856.

[4] Jayaraman S, Eswaran A, Rajagopal P, Palanisamy CP, Veerakumar P, Veeraraghavan VP, Sirasanagandla SR. Neuroendocrine-associated epigenetic factors in cellular senescence: mechanisms and therapeutic implications. Biogerontology. 2026; 27(2): 64.

[5] Ponnusamy B, Rajagopal P, Palanisamy CP, Veeraraghavan VP, Jayaraman S. Mechanistic Exploration of the anticancer activity of Justicia adhatoda Plant Leaf Ethanolic Extract against Colon Cancer Cells: An in silico and in vitro Approach. Asian Pacific Journal of Cancer Prevention. 2026; 27(3): 1069-1080.

[6] Pei J, Saran VS, Sivaramakrishnan R, Kanniappan GV, Pandurangan V, Jayaraman S, Dhayalan VK, Mironescu M, Mironescu ID, Palanisamy CP. Ultrasonic-assisted, Sargassum ilicifolium (brown marine macroalgae)-mediated biogenic synthesis of CuO nanoparticles incorporated in starch/PVA electrospun nanoscaffolds: In vitro safety and antioxidant efficacy assessment. Bioorganic Chemistry. 2026; 173: 109679.

[7] Raj MAPA, Subramaniyam S, Kanniappan GV, Jayaraman S, Palanisamy CP. Sustainable fabrication of starch/PVA/CuO electrospun nanoscaffolds from Turbinaria ornata (marine macroalgae) extract: Physicochemical characterization and antidiabetic evaluation. Kuwait Journal of Science. 2026; 53(2): 100545.

[8] Pei J, Ganesh NS, Subramaniyam S, Sivaramakrishnan R, Kanniappan GV, Jayaraman S, Palanisamy CP. Sustainable fabrication of starch/PVA/CuO electrospun nanoscaffolds from Padina tetrastromatica (Brown macroalgae) extract: Physicochemical characterization and antidiabetic assessment. Sustainable Chemistry One World. 2026; 9: 100195.

[9] Sakthiraj A, Sivaramakrishnan R, Subramaniyam S, Kanniappan GV, Pandurangan V, Jayaraman S, Dhayalan VK, Mironescu M, Mironescu ID, Palanisamy CP. Starch/PVA electrospun nanoscaffolds loaded with ultrasonic-assisted green-synthesis of CuO nanoparticles from marine macroalgae (Gracilaria corticata) extract: Cytotoxicity and antioxidant analysis. Chemical Physics Impact. 2026; 12: 101018.

[10] Raju M, Chandrasekaran MK, Loganathan L, Ahalliya RM, Mironescu M, Mironescu ID, Palanisamy CP, Kanniappan GV. Lipid remodeling and ferroptosis in phosphatidylcholine-mediated tumor–stroma crosstalk. Frontiers in Molecular Biosciences. 2026; 13: 1742305.

[11] Kunamalla R, Panagal M, Palanisamy CP. Biogenic synthesis and fabrication of starch/PVA/CuO electrospun nanoscaffolds from Sargassum ilicifolium (brown marine macroalgae) extract for anticancer activity on HT-29 and MCF-7 cancer cells. Biocatalysis and Agricultural Biotechnology. 2026; 72: 103923.

[12] Pei J, Govindaraj H, Sivaramakrishnan R, Kanniappan GV, Pandurangan V, Dhayalan VK, Mironescu M, Mironescu ID, Jayaraman S, Palanisamy PC. Sustainable fabrication of biopolymer-based (starch/PVA) nanoscaffolds loaded with green-synthesized CuO nanoparticles from Sargassum wightii (marine macroalgae): Cytocompatibility and antioxidant activity. Biomaterials Advances. 2026; 182: 214660.

[13] Pei J, Perumal NC, Meng P, Long Q, Palanisamy CP. Extracellular vesicle-based biosensors for Alzheimer's disease: A new frontier in precision diagnostics. Ageing Research Reviews. 2026; 113: 102904.

[14] Shree P, Sivaramakrishnan R, Kanniappan GV, Pandurangan V, Jayaraman S, Dhayalan VK, Mironescu M, Mironescu ID, Palanisamy CP. Antioxidant and biocompatible CuO-starch/PVA nanoscaffolds via ultrasonic green synthesis using Turbinaria conoides (brown marine macroalgae). Medicine in Drug Discovery. 2025; 28: 100238.

[15] Gong J, Lin J, Guan T, Pei J, Palanisamy CP, El-AtyFrom AMA. selenium tolerance to nanoplastic antagonism: Comprehensive characterization of L. casei SNUT1 and its extracellular vesicle–nanoselenium complex. Food Bioscience. 2025; 74: 107749.

[16] Poochi SP, Sundarraj R, Raju MV, Chandrasekaran MK, Ahalliya RM, Palanisamy CP, Kanniappan GV, Kondapavuluri BK, Thiruvengadam M. Harnessing Nature: Computational and Experimental Insights Into *Ipomoea obscura* Metabolites for Bladder Cancer Therapy. Chemistry and Biodiversity. 2025; 0: e00909.

[17] Dugganaboyana GK, Kannankumar MKG, Shivaramakrishna S, Raju MV, Chandrasekaran MK, Ahalliya RM, Panneerselvam N, Palanisamy CP, Kanniappan GV. Phytochemical insights, antioxidant activity and therapeutic potential of Cassia senna against prostate cancer in Wistar albino rats. Discover Applied Sciences. 2025; 7:1206.

[18] Natarajan SR, Krishnamoorthy R, Alshuniaber MA, Gatasheh MK, Rajagopal P, Veeraraghavan VP,

Palanisamy CP, Jayaraman S. KDM1A Facilitates Oncogenic Potential in Colorectal Cancer Progression Through the Activation of AXIN/GSK3β/β-Catenin Signaling Pathways: Evidence From Integrated Transcriptomics and In Vitro Studies. The Journal of Gene Medicine. 2025; 27(11): e70053.
[19] Guan T, Gong J, Lin J, Palanisamy CP, Jinjin Pei J, El-Aty AMA. Machine learning-driven multimodal optimization of selenium biotransformation and flavor profiling in fermented apple–Yacon functional beverages. Innovative Food Science & Emerging Technologies. 2025; 105: 104198.
[20] Natarajan PM, Umapathy VR, Murali A, Swamikannu B. (2022). Computational Simulations of Identified marine-derived Natural Bioactive Compounds As Potential Inhibitors of Oral Cancer. Future Science OA. 2022; 8(3).
[21] Natarajan PM, Umapathy VR. Role of transcriptomics in the study of oral cancer. Frontiers in Oral Health. 2025; 6:1524364.
[22] Vidhyarekha U, Natarajan PM, Bhuminathan S, Sabarinathan J, Suba R, Vijayalakshmi P. Role of artificial intelligence in Oral Cancer. Advances in Public Health. 2024. 2024: 3664408.
[23] Ganesan A, Kumar NG, Natarajan PM, Gauthaman J. Automated classification of elongated styloid processes using deep learning models-an artificial intelligence diagnostics. Frontiers in Oral Health. 2025; 5: 1424840.
[24] Umapathy VR, Natarajan PM, Swamikannu B. Regenerative Strategies in Dentistry: Harnessing Stem Cells, Biomaterials and Bioactive Materials for Tissue Repair. Biomolecules. 2025; 15: 546.
[25] Natarajan PM. Dental Bioinformnatics-Current Scope and Future perspectives. Research Journal of Pharmacy and Technology. 2022;15(5):2351-6.
[26] Ganesan A, Kumar NG, Natarajan PM. Solanum trilobatum leaf extract-derived silver nanoparticles downregulate the PI3K/AKT/mTOR signaling pathway and attenuate oral squamous cell carcinoma cell proliferation. Journal of Herbmed Pharmacology. 2024; 13(2): 300-307.
[27] Perumal MKK, Renuka RR, Subbiah SK, Natarajan PM. Artificial intelligence-driven clinical decision support systems for early detection and precision therapy in oral cancer: a mini review. Frontiers in Oral Health. 2025; 6: 1592428.
[28] Ramesh E, Ganesan A, Lakshmi KC, Natarajan PM. Artificial intelligence-based diagnosis of oral leukoplakia using deep convolutional neural networks Xception and MobileNet-v2. Frontiers in Oral Health. 2025; 6: 1414524.
[29] Ganesan A, Kumar NG, Natarajan PM. Anticancer activity of silver nanoparticles synthesized from aqueous leaf extract of Solanum trilobatum (Purple fruit pea eggplant) on human oral cancer cells. Journal of Herbmed Pharmacololgy. 2024; 13(2): 260-268.
[30] Natarajan PM, Swamikannu B, Sivaraman NM, Stylin AGSQ. Prevention of Oral Cancer: A Comprehensive Guide. Journal of Pharmacy and Bioallied Sciences. 2024; 16(5): S4239-S4241.
[31] Umapathy V, Dhanavel A, Kesavan R, Natarajan PM, Bhuminathan S, Vijayalakshmi P. Anticancer Potential of the Principal Constituent of Piper nigrum, Piperine: A Comprehensive Review. Cureus. 2024; 16(2): e54425.
[32] Umapathy VR, Swamikannu B, Natarajan PM, Devi R, Nandini MS, Vimalarani, Vijayalakshmi P. In Silico Molecular Docking of Ocimum sanctum Phytochemicals: Targeting Key Biomarkers in Oral Cancer. Journal of Pharmacy and Bioallied Sciences. 2024; 16(5): S4792-S4799.
[33] Natarajan PM, Bhuminathan S, Rajan R, Bindu K, Loganathan K, Veerakumar R. The Crucial Role of Smoking Cessation in Preventing Oral Cancer. Journal of Pharmacy and Bioallied Sciences. 2024; 16(5): S4245-S4247.
[34] Swamikannu B, Umapathy VR, Natarajan PM, Nandini MS, Stylin AGSQ, Vimalarani V, Rajinikanth S. Unlocking the Therapeutic Benefits of Artemisia Annua: A Comprehensive Overview of its Medicinal Properties. Journal of Pharmacy and Bioallied Sciences. 2024; 16(5): S4248-S4253.
[35] Natarajan PM. Computational Studies on Recent Congeners of Fluoroquinolones and Nitroimidazoles for Their Use in Periodontal Therapy. Journal of Pharmacy and Bioallied Sciences. 2024; 16(5): S4731-S4740.
[36] Yadalam PK, Arumuganainar D, Natarajan PM, Ardila CM. Artificial intelligence-powered prediction of AIM-2 inflammasome sequences using transformers and graph attention networks in periodontal inflammation. Scientific Reports. 2025; 15: 8733.
[37] Yadalam PK, Chatterjee S, Natarajan PM, Ardila CM. Comparison of light gradient boosting and logistic r egression for interactomic hub genes in Porphyromonas gingivalis and Fusobacterium nucleatum-induced periodontitis with Alzheimer's disease. Frontiers in Oral Health. 2025; 6:1463458.
[38] Natarajan PM, Bhuminathan S, Leela B, Bindu K, Loganathan K, Ramachandran V. Smoking and its Role in Oral Cancer. Journal of Pharmacy and Bioallied Sciences 16(5): S4242-S4244.
[39] Yadalam PK, Natarajan PM, Ardila CM. Variational graph autoencoder for reconstructed transcriptomic data associated with NLRP3 mediated pyroptosis in periodontitis. Scientific Reports. 2025; 15: 1962.
[40] Daniel Raja FS, Abraham L, Rangasamy K, Saikia K, Rathankumar AK, Mironescu M, Mironescu I, Palanisamy CP, Kanniappan GV. Next-Generation Microbiome Therapeutics: Psychobiotics and Fecal Microbiota Transplants (FMT) for Mental Health Treatment. Frontiers in Cellular and Infection Microbiology. 2026; 16: 1719357.

[41] Dharmaprakash S, Gunasekaran VP, Sivaramakrishnan R, Kanniappan GV, Jayaraman S, Mironescu M, Rajabathar JR, Mironescu ID, Palanisamy CP. Marine macroalgae-mediated ultrasonic-assisted green synthesis of CuO nanoparticles embedded in starch/PVA electrospun nanoscaffolds for in vitro α-amylase and α-glucosidase inhibitory activity. Scientific Reports. 2026.
[42] Natarajan SR, Krishnamoorthy R, Alshuniaber MA, Alsulami TS, Gatasheh MK, Rajagopal P, Palanisamy CP, Govindan R, Veeraraghavan VP, Jayaraman S. ABCE1 facilitates tumour progression via aerobic glycolysis and inhibits cell death in human colorectal cancer cells through the p53 signalling pathway. Scientific Reports. 2025; 15: 24674.
[43] Huang Y, Guo H, Liu Y, Jin W, Palanisamy CP, Pei J, Oz F, El-Aty AMA. Effects of Natural Polysaccharides on the Gut Microbiota Related to Human Metabolic Health. Molecular Nutrition & Food Research. 2025; 69:e202400792.
[44] Poornima K, Meenakshi K.C, Manikandan V.R, Shankari G, Prabhu D, Rathi M.A, Palanisamy CP, Balaji R, Gopalakrishnan V.K. Exploring the anticancer potential of Jerantinine A from *Tabernaemontana coronaria* against prostate, breast, and ovarian cancers: A computational approach. *Journal of Complementary and Integrative Medicine*, 2025 22(2): 363–372.
[45] Palanisamy CP, Poompradub S, Sansanaphongpricha K, Jayaraman S, Subramani K. Faridah Sonsudin gGreen synthesis of Nigella sativa-mediated silver nanoparticles for enhanced antibacterial activity and wound healing: Mechanistic insights and biomedical applications. Environmental Nanotechnology, Monitoring & Management. 2025; 24: 101085.
[46] Surendran N, Raju MV, Chandrasekaran MK, Ahalliya RM, Palanisamy CP, Chandrasekaran G, Kanniappan GV. Physicochemical characterization of starch from Maranta arundinacea L.(arrowroot) rhizomes and its inhibition of COX-2: In vivo validation. Bioactive Carbohydrates and Dietary Fibre. 2025; 33: 100465.
[47] Kannappan P, Chandrasekaran MK, Raju MV, Gopalakrishnan S, Dhamodharan P, Ahalliya RM, Palanisamy CP, Raju B, Kanniappan GV. Exploring the anticancer potential of Jerantinine A from Tabernaemontana coronaria against prostate, breast, and ovarian cancers: a computational approach. Journal of Complementary and Integrative Medicine. 2025; 22(02): 363-372.
[48] Pei J, Kumarasamy RV, Jayaraman S, Kanniappan GV, Long Q, Palanisamy CP. Quercetin-functionalized nanomaterials: Innovative therapeutic avenues for Alzheimer's disease management. Ageing Research Reviews. 2025; 104: 102665.
[49] Jayaraman S, Prasad M, Natarajan SR, Krishnamoorthy R, Alshuniaber MA, Gatasheh MK, Veeraraghavan VP, Rajagopal P, Palanisamy CP. Molecular mechanisms underlying the effects of beta-sitosterol on TGF-β1/Nrf2/SIRT1/p53-mediated signaling in the kidney of a high-fat diet and sucrose-induced type-2 diabetic rat. Chemico-Biological Interactions. 2025; 411: 111443.
[50] Huang Y, Guo H, Liu Y, Jin W, Palanisamy CP, Pei J, Oz F, El-Aty AMA. Effects of Natural Polysaccharides on the Gut Microbiota Related to Human Metabolic Health. Molecular Nutrition & Food Research. 2025; e202400792.
[51] Prabhakaran P, Palanisamy CP, Shanmugam A, Damodharan P, Swaminathan H, Devaraj D, Ahalliya RM, Kanniappan GV. Isolation, structural characterization, and molecular docking studies on the bioactive compound from n-Hexane extract of Emilia sonchifolia (L.) DC against the pancreatic cancer target Aurora 2 Kinase. Journal of Complementary and Integrative Medicine. 2024; 22(1): 0290.
[52] Jiang H, Kumarasamy RV, Pei J, Raju K, Kanniappan GV, Palanisamy CP. Integrating engineered nanomaterials with extracellular vesicles: Advancing targeted drug delivery and biomedical applications. Frontiers in Nanotechnology. 2024; 6: 1513683.
[53] Guo H, Liu Y, Wan T, Song D, Palanisamy CP, Geng J, Pei J, Özmen S, El-Aty AMA. Toward personalized cancer management: Role of precision nutrition–diet interventions. Journal of Functional Foods. 2024; 123: 106584.
[54] Natarajan SR, Krishnamoorthy R, Alshuniaber MA, Al-Anazi KM, Farah MA, Rajagopal P, Palanisamy CP, Veeraraghavan VP, Jayaraman S. Identification of FOXM1 as a novel protein biomarker and therapeutic target for colorectal cancer progression: Evidence from immune infiltration and bioinformatic analyses. International Journal of Biological Macromolecules. 282 (Part 4): 137201.
[55] Rajendran MS, Jayaraman S, Khan JM, Jasmine S, Prabhakaran RK, Raju MV, Chandrasekaran MK, Ahalliya RM, Kannappan P, Palanisamy CP, Kanniappan GV. Investigating the colon toxicity and carcinogenic role of monosodium glutamate compared with Dimethylhydrazine in male Wistar rats: Exploring the link to childhood colon cancer risk. Journal of King Saud University - Science. 2024; 36(11): 103507.
[56] Kumarasamy RV, Natarajan P, Umapathy VR, Roy JR, Rab SO, Saeed M, Panagal M, Mironescu M, Srinivasan GP, Palanisamy CP. Clinical Applications and Therapeutic Potentials of Advanced Nanoparticles: A Comprehensive Review on Completed Human Clinical Trials. Frontiers in Nanotechnology. 2024; 6:1479993.
[57] Jin W, Pei JJ, Roy JR, Jayaraman S, Ahalliya RM, Kanniappan GV, Mironescu M, Palanisamy CP. Comprehensive review on single-cell RNA sequencing: A new frontier in Alzheimer's disease research. Ageing Research Reviews. 2024; 274: 102454.

[58] Pei J, Palanisamy CP, Jayaraman S, Natarajan PM, Umapathy VR, Roy JR, Panagal M, Jayaraman S. Curcumin-loaded polymeric nanomaterials as a novel therapeutic strategy for Alzheimer's disease: A comprehensive review. Ageing Research Reviews. 2024; 99: 102393.
[59] Pei J, Palanisamy CP, Jayaraman S, Natarajan PM, Umapathy VR, Roy JR, Thalamati D, Ahalliya RM, Kanniappan GV, Mironescu M. A comprehensive review on starch-based Sustainable Edible Films Loaded with Bioactive Components for Food Packaging. International Journal of Biological macromolecules. 2024; 274 (Part-1): 133332.
[60] Palanisamy CP, poompradub S, Sansanaphongpricha K, Subramani K, Sonsudin F. Increased expression levels of PDGF and VEGF magnify the wound healing potential facilitated by biogenic synthesis of silver nanoparticles. Nano-Structures & Nano-Objects. 2024; 39: 101236.
[61] Pei J, Palanisamy CP, Jayaraman S, Natarajan PM, Umapathy VR, Roy JR, Thalamati D, Ahalliya RM, Kanniappan GV, Mironescu M. Proteomics Profiling of Extracellular Vesicle for Identification of Potential Biomarkers in Alzheimer's Disease: A Comprehensive Review. Ageing Research Reviews. 2024; 99: 102359.
[62] Xi J, Wang T, Xian P, Liu X, Du M, Yang H, Palanisamy CP, Lin W, Long Q. Proteomic insights uncover enhanced neurotherapeutic potential in conditioned mesenchymal stem cell-derived extracellular vesicles. Extracellular Vesicle. 2024; 3: 100037.
[63] Pei J, Natarajan PM, Umapathy VR, Swamikannu B, Sivaraman NM, Krishnasamy L, Palanisamy CP. Advancements in the synthesis and functionalization of zinc oxide-based nanomaterials for enhanced oral cancer therapy. Molecules. 2024; 29(11): 2706.
[64] Gatasheh MK, Natarajan SR, Krishnamoorthy R, Alsulami TS, Rajagopal P, Palanisamy CP, Veeraraghavan VP, Jayaraman S. Molecular analysis to identify novel potential biomarkers as drug targets in colorectal cancer therapy: an integrated bioinformatics analysis. Molecular and Cellular Oncology. 2024; 11(1): 2326699.
[65] Pei J, Yan Y, Jayaraman S, Rajagopal P, Natarajan PM, Umapathy VR, Gopathy S, Roy JR, Sadagopan CS, Thalamati D, Palanisamy CP, Mironescu M. A review on advancements in the application of starch-based nanomaterials in biomedicine: Precision drug delivery and cancer therapy. International Journal of Biological Macromolecules. 2024; 130746.
[66] Pei JJ, Yan Y, Palanisamy CP, Jayaraman S, Natarajan PM, Umapathy VR, Gopathy S, Roy JR, Sadagopan JC, Thalamati D, Mironescu M. Materials-based drug delivery approaches: Recent advances and future perspectives. Green Processing and Synthesis. 2024; 13: 20230094.
[67] Pei JJ, Deng W, Liu Y, Guo Y, Chen J, Abdu H, Khan MR, Palanisamy CP, El-Aty AM. A Comprehensive Review of Cornus officinalis: Health Benefits, Phytochemistry, and Pharmacological Effects for Functional Drug and Food Development. Frontiers in Nutrition. 2023; 10: 1309963.
[68] Alugoju P, Palanisamy CP, Anthikapalli NVA, Jayaraman S, Prasanskulab A, Chuchawankul S, Dyavaiah M, Tencomnao T. Exploring the anti-aging potential of natural products and plant extracts in budding yeast Saccharomyces cerevisiae: A review. F1000Research. 2023; 12: 1265.
[69] Lavanya M, Krishnamoorthy R, Alshuniaber MA, Manoharadas S, Palanisamy CP, Veeraraghavan VP, Jayaraman S, Rajagopal P, Padmini R. Formulation, characterization and evaluation of gelatin-syringic acid/zinc oxide nanocomposite for its effective anticancer, antioxidant and anti-inflammatory activities. Journal of King Saud University-Science. 2023; 35: 102909.
[70] Palanisamy CP, Poompradub S, Sansanaphongpricha K, Jayaraman S, Subramani K, Sonsudin F. Biosynthesis of silver nanoparticles (AgNPs) using ethanolic extract of Nigella sativa (L.) seeds promotes wound healing via PDGF and VEGF signalling pathways activation. Biocatalysis and Agricultural Biotechnology. 2023; 54: 102970.
[71] Prasad M, Jayaraman S, Natarajan SR, Veeraraghavan VP, Krishnamoorthy R, Gatasheh MK, Palanisamy CP, Elrobh M. Piperine modulates IR/Akt/GLUT4 pathways to mitigate insulin resistance: Evidence from animal and computational studies. International Journal of Biological Macromolecules. 2023; 253: 127242.
[72] Palanisamy CP, Pei JJ, Phaniendra A, Venkata AAN, Jayaraman S, Veeraragahavan VP, Sridevi G, Roy JR, Janaki CS, Thalamati D, Mironescu M, Luo Q, Chai Y, Long Q. New Strategy of Neurodegenerative Disease Treatment with Extracellular Vesicles (EVs) Derived from Mesenchymal Stem Cells (MSCs). *Theranostics*. 2023; 13(12):4138-4165. doi:10.7150/thno.83066.
[73] Palanisamy CP, Phaniendra A, Jayaraman S, Poompradub S. *Nigella sativa* L. seed extracts promotes wound healing progress by activating VEGF and PDGF signalling pathways: *An in vitro* and *in silico* study. *F1000 Research*. 2023; 12: 436.